Chapter 4

Edge Detection in Primate Visual Cortex

4.1 Introduction

Visual stimuli are initially processed in the primary visual region (V1) of the cerebral cortex. Area V1 contains a detailed map of the eyes' total field of vision. Rods, responsible for scotopic vision, and cone receptor cells, responsible for color vision, trap and transmit light stimuli in the retina. The responses from these photo-transducers are either funneled to the bipolar cells (BC) or are routed through the horizontal cells. ON and OFF bipolar cells configurations transmit transduced signals from the photoreceptor cells to the ganglion cells for signal interpretation in learning and cognition. Hubel and Wiesel discovered the essential attributes of the primary visual cortex by recording electrical activity in animal experiments. They published landmark scientific articles on V1's cellular responses, anatomy, development, and connectivity, later used in the theory of simple and complex cells, beginning in the 1950s. Simple filtering to improve edges and contours is the primary operation that V1 conducts on visuals. It is believed that simple cells carry out linear filtering, which is characterized as weighted sums of an image's intensity values, with the weights being decided by the receptive field (RF) profile. Complex cells adds the rectified outputs of simple cells responses, computing an image's overall energy in a frequency and orientation band. The primary activity V1 carries out on images before transmitting them to succeeding layers of the visual cortex is assumed to be simple filtering to improve edges and contours, which then allows for the performance of complicated operations like cognition and learning. Interpretation of signal transduction in the visual cor-

tex and translation of transduced signals for pattern extraction as a function of the RF by individual neurons has not been explored beneath these computational paradigms of complex neuronal networks.

4.1.1 Research Gap

Moreover, the role of individual neuron morphology, differential active ion distribution, and electrophysiology in shaping complex neuronal responses is still unknown. There are undiscovered links between local neuron dynamics and their role in influencing global responses due to the unavailability of precise measuring devices. Previous literature treats dendrites as spatio-temporal acquisition and weighted connectome-based learning units, and the cell body as a computational unit responsible for non-linear integration of cumulative signals. However, the diversity in the morphology of neurons, their connectome specificity, and differential distribution of active ion channels in dendritic arbor describes these versatile computational units to be much more complex. Recent discoveries in the field have revealed new dimensions in system neuroscience, linking complex function formation, cognition, and memory to neuronal morphology, local structural dynamics, and temporal encoding, in conjunction with neuron connectome specificity and non-linear activation function. Understanding the local processes associated with the fundamental components of neurons and linking those elementary faculties to local as well as global responses will aid in bridging the gap between existing in-vivo discoveries and their potential role in structure-function relationships in systems neuroscience.

4.1.2 Related Works

Ramon y Cajal [179] introduced significant literature and detailed morphological structures in terms of dedicated circuits organized in the primate visual cortex (PVC). A diverse set of neuronal morphologies arranged in multiple layers with dedicated functionalities aimed at improving cognition, plasticity, and learning tasks. These complex functionalities are suggested to be achieved by reorganizing connections [180], and growing and retracting dendritic inputs [181]. Hubel and Wiesel proposed the basic floor plan of the mammalian retina [182–185], in which localized neurons transduce light signals and encode them into orientation-selective (OS) spiking responses in primary layers. In contrast, scale and location-independent cognition occur in others. The primary V1 layers of the visual cortex

compute these OS responses, which appear to be the foundation of mammalian visual perception and cognition. Based on these preliminary studies, a relatively small amount of work has been published to replicate localized behavior in the areas of orientation selectivity [186, 187], scale and position-independent cognition [188, 189], and learning [188, 189]. The importance of neuronal anatomy and physiology in functional computation in orientation selectivity and other complex functionality has been highlighted in the literature. But connectome structure [123, 190–192], the role of unique neuronal morphologies [193, 194], and the dynamics of such morphologies due to localized active ion channels [137, 138, 141, 195] remains poorly defined. Recent works [123, 191] confirm single-cell precision microarchitecture in the mammalian visual cortex, while literature [137, 138, 195] describes dynamics of neuronal inputs (dendritic arbors) as being dependent on localized active ion channels. Ganglion cells are believed to play a crucial role in the orientation selectivity of edge information received by the PVC. *But how accurately is the edge information being perceived by the visual cortex, and how are these patterns being generated at the sub-cellular level?* The fundamental question pertains to the link between the functional role of a diverse collection of a precisely organized modular parasol and midget cell morphologies with sub-cellular active ion channel distribution and direction as well as orientation selectivity. Missing links between localized ion channels and dendritic morphologies attracts interest in understanding the role of differential sub-cellular active ion distribution within ganglion cell dendritic morphologies in shaping direction/orientation selectivity [139, 142].

4.1.3 Aim

The goal of this chapter is to mathematically model and replicate the neuronal dynamics of OS RGC by combining active and passive fiber neuronal dynamics, that are proposed in the previous chapter. The RGC has been modeled to mimic local dynamics resulting from the differential distribution of localized AICs in the dendritic arbor, and it has been linked to the RGC's orientation selectivity response as a function of neuron morphology and localized active ion channel distribution, as well as connectome specificity. The modeled responses of OS-RGC networks have been compared to state-of-the-art neural network models for edge detection. Another aim of this chapter is to simulate a neuronal network of OS-RGC layer behavior in the striate cortex V1 layer of the PVC and the probable application of such network in edge detection in an uncoupled as well as coupled network.

4.1.4 Contribution

The proposed framework of modeling and simulation of scotopic and color vision model and its implication in edge-map estimation gives a clear understanding of the local processes contributing to global responses.The model response suggests the neuron morphology and physiology to play an important role in structure-function relationship. Model design and simulation of orientation selective RGC layer shows very consistent responses in terms of preferred orientation specificity as discussed in Hubel and Weisel. Comparison of our model with state-of-art literature shows accuracy of the proposed model proportionate to actual human edge-estimation performances. On the other hand, integrating the coupled fiber model with the scotopic vision model suggests bandwidth tuning and complex function relation due to cell-field interaction.

4.2 Striate Cortex of the Primate Visual Cortex

The V1 layer of the visual cortex influences the first stage of information perception. The V1 layer has a very well-defined map of spatial information in vision (the retinotopic map). A substantial percentage of V1 is mapped to the small, central portion of the visual field in humans and animals with a fovea (cones and rods in the retina), a method known as cortical magnification. V1 neurons may have the smallest RF size (i.e., the highest resolution) of any visual cortex microscopic region, possibly for the objective of accurate spatial encoding. Individual V1 neurons in humans and animals with binocular vision have ocular dominance, which means they tune to one of the two eyes. Neurons with comparable tuning characteristics frequently form cortical columns in V1 and the primary sensory cortex as a whole. For two tuning qualities, ocular dominance and Orientation, David Hubel and Torsten Wiesel suggested the traditional ice-cube organization model of cortical columns. However, this model is unable to account for the colour, spatial frequency, and numerous other characteristics to which neurons are tuned. The goal of this study is to develop models for interpreting visual data as it is most likely perceived by a single layer of the primary visual cortex. Two distinct neuron morphologies organized in precise repetitive micro-architecture have been incorporated [191, 192, 196], as well as distinct cell physiology and dynamics of each neuron with localized ion channels [180, 197, 198]. The model's input is analogous to the response of BC (ON and OFF) to light intensity. The output of the network is analyzed in terms of the firing rate of neurons to approximate an over-

all understanding of visual representation in a single layer of the primary visual cortex's neuronal network, and this response is feed-forward to a single layer of OS-RGC. The efficacy of edge detection performances reconstructed from four OS layers of the RGC network has been compared using quantitative and qualitative analysis of responses from the proposed architecture. The model is inspired by the architecture of the PVC, and the process of transduction of light stimuli into neuro-modulated signals mimic attributes of different cells associated with the modeled network, such as the BC and the RGCs. Figure4-1 depicts the topology of the primates' visual cortex, in which light stimulation is trapped by photoreceptor cells (rod and cone cells) and transduced to localized spatio-temporal signals. Color vision, responsible for frequency discrimination and scotopic vision, responsible for night vision, has been considered to investigate their role in edge perception. The transduced Spatio-temporal signals are subsequently relayed directly or indirectly to the ON and OFF BC, which later form the basis of RFs. In the subsequent sections, the model's architecture, interconnections between distinct cells, neuron morphology employed in the model, and connectome specificity of RGC neurons with BC are discussed in detail.

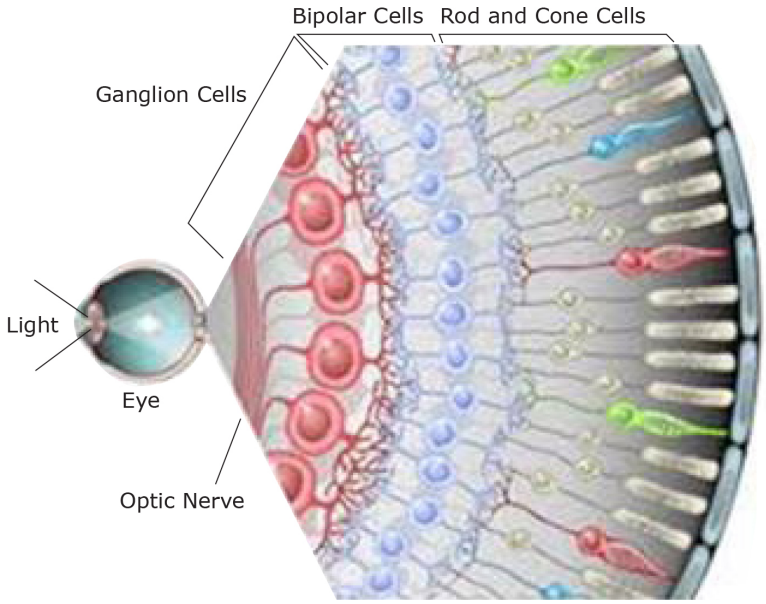

Figure 4-1: As demonstrated in [1], the organisation of distinct cells from photoreceptors to the RGC network, as well as the relevant sections, are taken into account while modelling the suggested single layered network of visual cortex.

4.3 Model Architecture

The primate retina is about 0.5 *mm* thick over most of its length, with three layers of cell bodies and two layers containing synaptic interconnections between neurons. The fovea, a specialized region of the primate retina near the optical axis of the eye, is made up of a single layer of neurons, the photoreceptor cells. Other neurons send input to the dendritic fields, and the axon, which can branch, carries the neuron's output to its destination. Some neurons lack an axon and only influence synapses within the dendritic field through local interconnections. The shape of a neuron's dendritic field and axonal branches are both important features in identifying different types of neurons. To classify and understand retinal neurons, a variety of features and attributes are necessary, such as the locations of cell bodies, dendrites, and axons; the size and shape of their cell bodies and dendritic fields; and their interconnections with other neurons.

Retinal neurons are divided into five categories, each of which has several sub-categories. The location of cell bodies, dendritic fields, and axon terminals distinguish the major categories of retinal neurons. The cell bodies of photoreceptors are found in the layer's outer nuclear layer. The photoreceptors' synaptic terminals make contact with the bipolar and horizontal cells' dendritic fields in the outer plexiform layer. The bipolar and horizontal cells' cell bodies are found in the inner nuclear layer. Horizontal cells' dendrites and branching axon terminals make connections with cells in the outer nuclear layer, and connectome specificity with the type of BC with RGC forms the basis of RFs.

The proposed model takes into account topology in neuronal cell arrangements and connectivity with BC. The proposed model has three major components. Firstly the input layer, which is responsible for processing light stimuli and translating them into Spatio-temporal signals that are in turn fed to the BC. Secondly, the connection-specific RGC network, which is responsible for orientation estimation from the visual scene. Thirdly, the rate encoder, which is responsible for the conversion of Spatio-temporal data into spatial information for descriptive and inferential statistical purposes. The following sections delve into the specifics of the three layers.

4.3.1 The Input Layer

The first layer of the visual cortex is the input layer, which is responsible for trapping light stimulation and converting spatial information into temporal data. The photoreceptor cells are located at the beginning of the input units and are responsible for transforming light stimuli into temporal electric signals for sensing and processing by the visual cortex. The majority of the retina contains two types of photoreceptor cells: rod photoreceptor cells for scotopic vision and cone cells for color vision. Rod cell density is significantly higher than cone cell density and is responsible for high-resolution information such as textures and fine features.

The proposed approach emphasizes on the modeling of signal representation in BC and their potential application in edge detection. The ON-bipolar cells (ON-BC), which are sensitive to light intensities, are connected directly to photoreceptors, or the OFF-bipolar cells (OFF-BC) via the horizontal cells, which are sensitive to darkness intensities. To mimic the behavior of photoreceptor cells, natural images in 'jpeg,' 'png,' and 'tiff' are used as visual stimulation, that are fed to BC for the processing of visual information.

4.3.1.1 Photoreceptors

Light (visible electromagnetic radiation) is converted into responses by photoreceptors, which is used to stimulate biological processes. Rods and cones cells are the two types of photoreceptor cells found in mammals' eyes. Cones require much brighter light to produce a signal than rods, which are incredibly sensitive and can be triggered by just one photon. The likelihood of their respective photo-receptor proteins absorbing photons of different wavelengths determines the different responses of the three types of cone cells (L, M, and S-cones). As a result of cone cells' wavelength dependence, color perception is more difficult in low-light conditions, and humans have scotopic vision dominance during night vision. Rod cells, on the other hand, are highly sensitive to light intensity and contrast and can detect single photons, making them important in scotopic vision.

The proposed framework is based on biological vision processing. The model's input is either a gray-scale image with scene intensity information transduced by photoreceptor cells in scotopic vision or a color image with 'Red,' 'Green' and 'Blue' frames to 'L-cones,' 'M-cones' and 'S-cones' respectively depicting the spectral frequency dependence. These transduced signals from the rod and cone cells are then fed to the BC layer, which mimics the behavior of suitable BC and

serves as the foundation for RGC cell RFs and response generation.

4.3.1.2 Bipolar Cells

In the retina, BCs are located between photoreceptors and ganglion cells. They act, directly or indirectly, to transmit signals from the photoreceptors to the ganglion cells. The BC receive the signals either directly from the photo-receptors or via the horizontal cells and pass them on to the ganglion cells directly or indirectly (via amacrine cells). BCs receive synaptic input from either rods or cones or both rods and cones. Rod BC do not synapse directly onto ganglion cells. Instead, rod BC synapse onto a Retina amacrine cell, which in turn excite cone ON-BC (via gap junctions) and inhibit cone OFF-BC (via glycine-mediated inhibitory synapses). These cells overtake the cone pathway in order to send signals to ganglion cells at scotopic (low) ambient light conditions. The mechanism for producing the monochromatic surround of the same RF, on the other hand, is being studied. It is suggested that the horizontal cell plays an important role in the process, the exact sequence of receptors and molecules is unknown.

The model emphasizes two types of BCs, namely the ON-BC and the OFF-BC responses to orientation selectivity. BCs are chosen based on their sensitivity to light or darkness, which are then linked to photoreceptor cells in scotopic vision. Gray intensity images are taken to mimic the contrast and intensity dependence in the case of night vision.

A similar approach has been undertaken to mimic color vision in the retina. In the case of color vision, 'Red,' 'Green,' and 'Blue' frames of the color image are used to mimic their spectral frequency dependence.

ON-BC, which are directly connected to photo-receptor cells, respond to the localized spatial light intensity with sustained depolarization and darkness with sustained hyperpolarization, and vice versa for OFF BC [199–202]. Sustained depolarization or hyperpolarizations produced by the BCs are modeled as temporal rectangular current pulses with amplitudes proportional to spatial intensities. The length of the temporal current pulses generated by the BCs is taken as 350 $mSec$ with an offset of 10 $mSec$ and a pulse width of 240 $mSec$. Given the average visual response sensitivity of primate vision, the time duration of the temporal signal is taken as 350 $mSec$ with a pulse width of 240 $mSec$. These current pulse responses from BCs, as shown in Figure4-2 and Figure4-3 are fed as input to the RGCs [186, 203]. Their effects on the post-synaptic neuron are modeled as linear

in terms of spiking frequency. The magnitude of persistent depolarization and hyperpolarization corresponding to light or darkness is scaled within the range of -128 *to* 127 nA current by a factor of 8. The BCs transform the incoming signals within the sensitivity range of the connected RGCs [204–206].

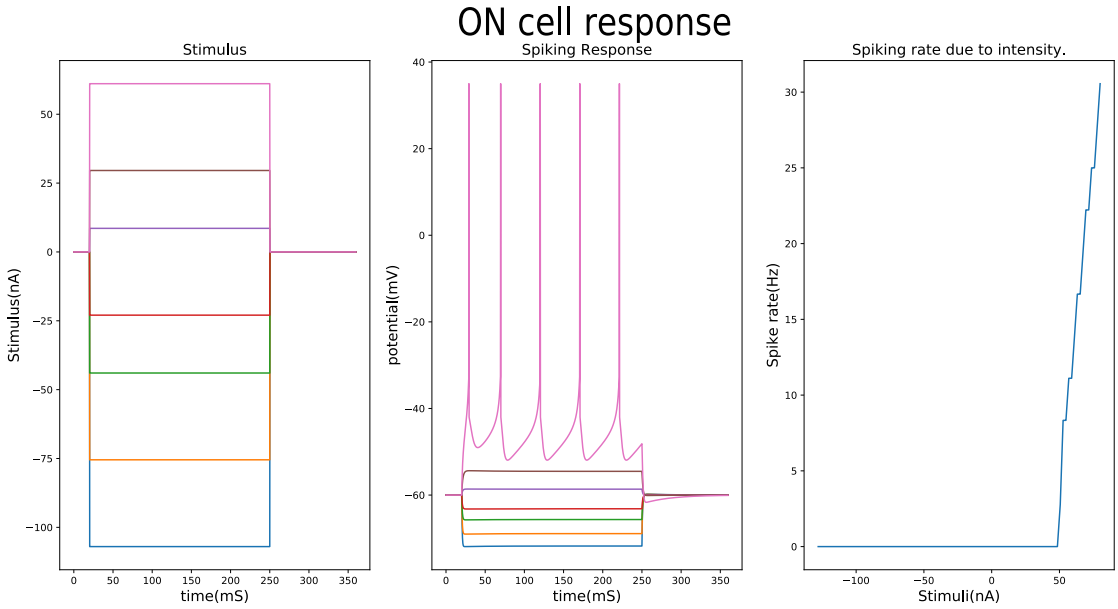

Figure 4-2: ON-BC response is encoded as square pulses (sustained depolarization or hyperpolarization) due to light intensity transduction, fed to the post synapse of the RGCs, and the corresponding spike rates.

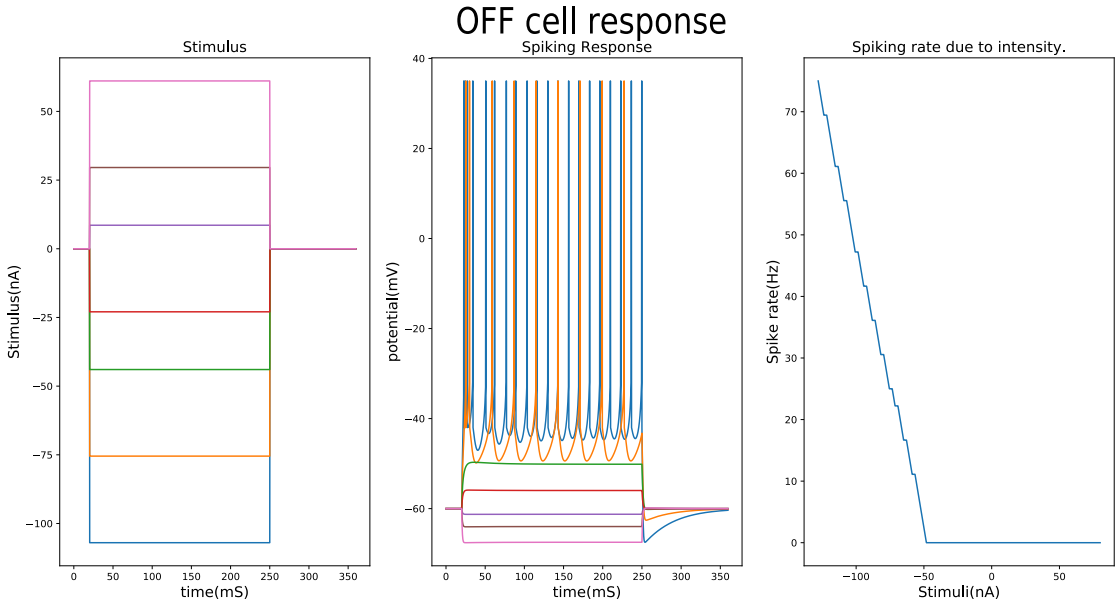

Figure 4-3: OFF-BC response is encoded as square pulses (sustained depolarization or hyperpolarization) due to light intensity transduction, fed to the post synapse of the RGCs, and the corresponding spike rates.

Shown in Figure4-2 and Figure4-3 are the temporal responses generated from the trapped stimuli fed to the ON-BC and OFF-BCs, respectively, corre-

sponding to localized spatial stimuli to photoreceptors in the retina. ON-BCs are sensitive to light stimuli and depolarize the membrane potential corresponding to the amplitude of light and hyper-polarize the membrane potential corresponding to the amplitude of darkness and vice versa in the case of OFF-BCs. Mathematical simulations of BC responses are computationally expensive. Conversion of localized spatial information into time-series BC response of 350 $mSec$ length with a quantization factor of 0.01 $mSec$ and integrating electrophysiological and electro-chemical attributes significantly affects the computational complexity of the proposed methodology. To optimize the computational complexity of the proposed model, BC responses are taken as square pulses of pulse width 240 $mSec$ with an offset of 10 $mSec$ and total simulation signal length of 350 $mSec$ and pulse amplitude directly proportional to the intensity of the localized visual stimuli.

4.3.2 The Processing Layer

Spatio-temporal signals from the BCs are fed to the anatomically distinct RGC cells arranged in modular, distinct repetitive patterns with the BCs. The RGC cell with distinct connectome specificity processes the cumulative signals to extract orientation-selective information. Connectome specificity of the proposed model, as well as electrophysiological and electro-chemical attributes of the anatomically distinct RGCs with localized AICs, have been presented in detail in the subsequent sections.

4.3.2.1 Retinal Ganglion Cell Morphology

A retinal ganglion cell (RGC) is a type of neuron found near the inner surface of the retina (the ganglion cell layer). It receives sensory input from photoreceptors through two types of intermediary neurons: BCs and retina amacrine cells. Retina amacrine cells, particularly narrow field cells, are critical for forming functional subunits within the ganglion cell layer and allowing ganglion cells to detect a small dot moving a short distance. On the other hand, RGCs connected to BCs are reported to be associated with orientation information, contour detection, and other such pattern extraction processes utilized in recognition and learning. RGCs jointly transfer image-forming and non-image-forming visual information from the retina to numerous locations in the thalamus, hypothalamus, and mesencephalon, or midbrain, in the form of AP. RGCs differ substantially in terms of size, connections, and responses to visual stimulation, but they all have a long axon that goes

into the brain. These axons are responsible for the formation of the optic nerve, optic chiasm, and optic tract. Despite the fact that much has been studied about the different layers of the visual cortex over the last few decades in an attempt to comprehend the identical properties of such layers, little has been studied about individual neuron features and functionality, the importance of neuronal anatomy and morphology corresponding to the RGC cells, and their role in local function formation and global responses.

Two unique morphologies for RGCs have been designed and examined in the proposed model to compare the differences in computing functionality. The morphology of the neurons and their corresponding connection matrices are based on the well-known 'Sobel edge' detector and directed gradient kernels. As demonstrated in Figure4-4a and Figure4-4b, one cell has a less arborized morphology with 4 dendritic terminals communicating with ON and OFF BCs synonymous to RGC with a small RF, while the other has 6 dendritic terminals contributing to neuronal computation depicting an RGC with the comparatively larger RF.

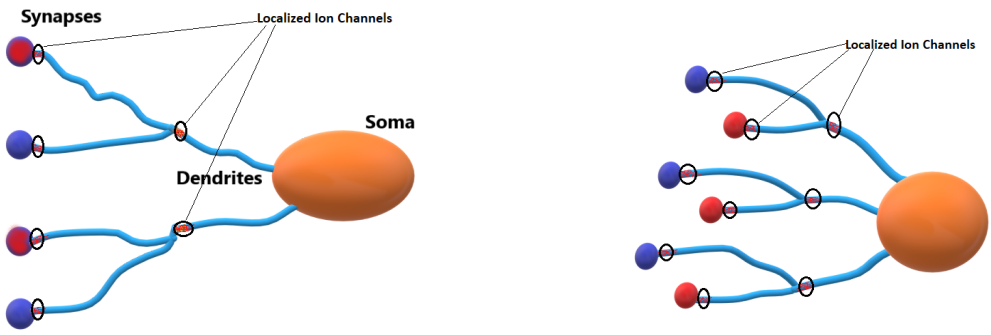

(a) **(b)**

Figure 4-4: Two distinct morphology of RGCs were used in the proposed work. **(a)** Midget RGC with 4 dendritic terminals connecting to the ON and OFF-BCs, **(b)** RGC with 6 dendritic terminals connecting to ON and OFF-BCs.

The red synaptic connections are connected to ON-BCs while the blue terminals are attached to OFF-BCs of the corresponding photoreceptor cells, as shown in Figure4-4a and Figure4-4b. Dendritic junctions, cell body, and post-synaptic connections are rich in active ionic channel concentration at localized regions [137–139, 141, 142] and are suspected of triggering non-linear membrane dynamics due to the cumulative propagating signals. These non-linearities in localized regions of the RGC are modeled using the 'bursting,' 'chattering,' and 'regular spiking' type of membrane dynamics [204–207]. Izhikevich's 'bursting'

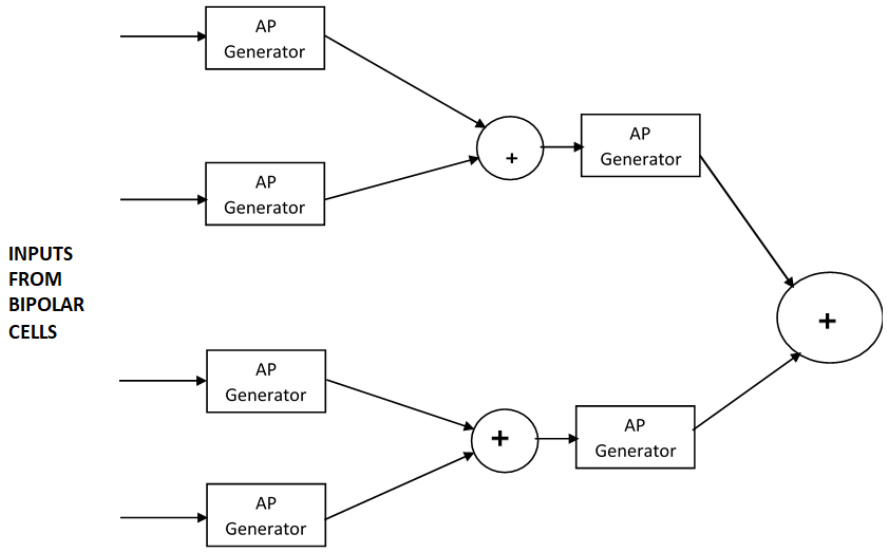

Figure 4-5: Functional aspect of the neuron in Figure.4-4a.

or 'chattering' type of membrane dynamics are integrated because of its proficiency in mimicking calcium dynamics and their relevance in primates' visual cortex. Combinations of types of active ion channels at specific locations control the bandwidth of the connected RGC. Appropriate combinations of 'chattering' and 'bursting' membrane localization give the RGC high-pass filter or a band-pass filter type of behavior by controlling the overall axial current delivered to the successive nodes. The rest of the dendritic fiber is passive and is partitioned into isopotential compartments to aid decremental conduction [208]. In Figure4-5, the analogous neuron function of the RGC in Figure4-4a is presented. As stated in [204–207], the parameters for spiking activity have been chosen. The propagation delay caused by propagation through passive fibers is ignored, and the propagating signal from distal dendritic fibers reaches the daughter branches, parent branches, the junctions, and the soma coherently. As the sensed stimuli propagate through the dendritic arbor to the cell body, the cumulative responses at the junction of dendritic branching are renewed and re-encoded attributed to the prevalence of localized AICs, and the process repeats itself until the propagating signal reaches the cell body. At the cell body of the RGC neuron, the total responses due to cumulative propagating current from the entire dendritic arbor are summed and reprojected in terms of spiking frequency.

4.3.2.2 Connectome Specificity of RGCs with Bipolar Cells

Connectivity of BCs with the RGC network forms the basis of RFs and is suspected to be the core of differential of gradient (DoG) function type responses in the

primate's primary visual cortex. The width of the dendritic spread of RGCs corresponds to different sizes of RFs, with small RFs corresponding to RGC in Figure4-4a and larger RFs due to RGC in Figure4-4b cell connectivity. Small and large RFs due to different dendritic spread in Figure4-6a and Figure4-6b within a neighbourhood of 3×3 grid BCs corresponding to Figure4-4 and connectivity Figure4-7 and Figure4-8 has been shown in Figure4-6.

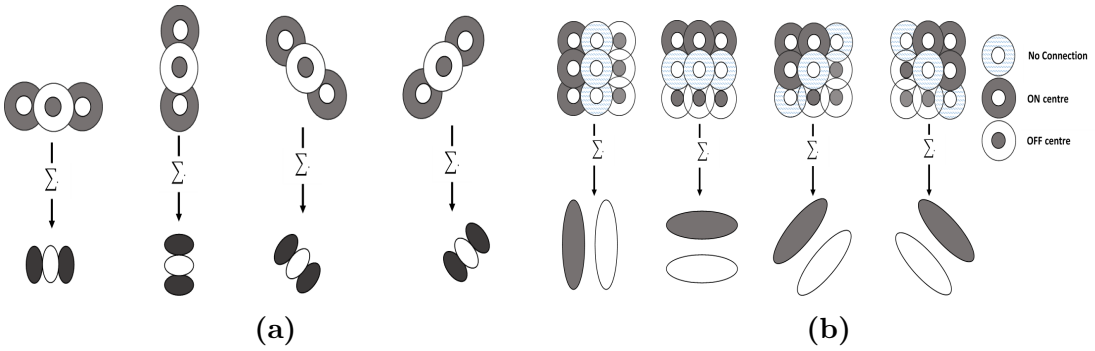

Figure 4-6: RFs connectome specificity for 3×3 grid of RGC in Figure4-4 cell connectivity. **(a)** RF due to RGG dendritic spread in Figure4-4a connectivity corresponding to 4 selective orientation and **(b)** RF due to RGC dendritic spread in Figure4-4b connectivity corresponding to 4 selective orientation.

RFs in the visual and somatosensory systems could be fundamentally circular or oval portions of the retina or skin. Visual and somatosensory RFs of the thalamus, on the other hand, are circular and display center-surround antagonism, in which the initiation of a stimulus in one cutaneous or retinal region triggers activating responses and in surrounding regions evokes inhibiting effects. As a result, the identical stimulus elicits opposing reactions in those locations. The effects of stimulus antagonism at several locations are a manifestation of a phenomenon known as lateral inhibition. The ideal stimulation in lateral inhibition is not uniformly distributed across the RF but rather a discrete stimulation with the contrast between center and surrounding locations.

0	1	0
0	-1,-1	0
0	1	0

0	0	0
1	-1,-1	1
0	0	0

0	0	1
0	-1,-1	0
1	0	0

1	0	0
0	-1,-1	0
	0	1

Figure 4-7: Connectivity matrices for detection of four directional edges namely vertical, horizontal, and two diagonal components from left hand side to the right right hand side respectively for neuron model in Figure4-4a and RFs corresponding to Figure4-6a.

In the proposed methodology, these RFs are constructed by connecting RGC cells in modular patterns with RF formations as shown in Figure4-6a corresponding to RGC shown in Figure4-4a and Figure4-6b corresponding to RGC

morphology shown in Figure4-4b. As described in [209], the connectivity of non-sister dendrites of RGCs with ON or OFF BCs is convergent. Each RGC is constructed in precise modular repeated structures, as seen in Figs. 4-7 and Figure4-8. Each neuron is distributed throughout a 3×3 grid of BCs (both ON and OFF), where 1 signifies connectivity with an ON-BC and -1 specifies connectivity with an OFF-BC, which is then coupled to the equivalent pixel representation of photoreceptor cells. Two $-1's$ in the center pixel of Figure4-7 indicate interconnectivity of two dendritic branching in the central OFF-BC, while 0 indicates no connectivity with the corresponding BCs.

1	1	1
0	0	0
-1	-1	-1

-1	0	1
-1	0	1
-1	0	1

0	1	1
-1	0	1
-1	-1	0

1	0	0
0	-1,-1	0
	0	1

Figure 4-8: Connectivity matrices for detection of four directional edges namely vertical, horizontal, and two diagonal components from left hand side to the right right hand side respectively for neuron model in Figure4-4b and RFs corresponding to Figure4-6b.

Similarly in case of the connectivity martix shown in Figure4-8, corresponds to the connectity matrix of corresponding to the RGC morphology shown in Figure4-4b cell, '1' in the conectivity matrix signifies excitatory connectivity of RGC with corresponding localized ON-BC, '-1' in the conectivity matrix signifies inhibitory connectivity of RGC with corresponding localized OFF-BC and '0' represents no connectivity. Connectivity neighbourhood of RGC controls the size of RFs that in turn controls the spatial resolution of the RGC. RGC modules are connected in repetitive patterns over the BC layer to form RGC network layer.

4.3.2.3 Modeled Functions of Dendritic fibers, Junctions, and Soma

The amplitude of the ON/OFF BC response, which in turn transduces the strength of light stimuli into a change in membrane potential and spike encoding in those localized regions, is required for excitation and hyper-polarization in localized active regions of the dendrites near the post-synaptic terminal. Izhikevich membrane model [2, 205, 206] is integrated for mimicking calcium dynamics such as 'regular spiking', 'bursting' and 'chattering' type of spiking activity and is computationally simple. Because of its capability to mimic a wide range of spiking dynamics and computational simplicity, the membrane dynamics in these regions are modeled using the 'Izhikevich' spiking neuron model. The membrane dynamics regulating

the spiking activity in localized active ion channels are given as:

$$C\frac{dv}{dt} = k\left((v - v_r)(v - v_t) - u + I\right), \quad if\ v \geq v_t \tag{4.1}$$

$$\frac{du}{dt} = a\left[b(v - v_r) - u\right], \qquad v \leftarrow c, u \leftarrow u + d \tag{4.2}$$

where 'v' stands for "membrane potential," 'I' for "neuronal stimuli," 'u' for "recovery current," 'v_r' for "resting membrane potential," and 'v_t' for "threshold potential." The parameters a, b, c, d, k, C regulates different spiking activities and has been discussed in details in [2, 3]. In the proposed work spiking parameters corresponding to bursting and chattering activity has been used to mimic dynamics due to calcium ion channels in the visual cortex and other cerebellar region and the parameter values for the Izhikevich membrane model has been given in Table.4.1.

Table 4.1: Izhikevich propagation and bursting membrane parameters taken from [2, 3].

Izhikevich Parameter	Bursting Parameter	Chattering Parameter	Propagation Parameter	Value
a	0.01	0.03	C_m	1μF
b	5	-2		
c	-56	-50	R_{lon}	2Ω
d	130	100		
C	150nF	100nF	ϵ_L	-65mV
k	1.2	0.7		
v_r	-65mV	-60	G_L	10^{-6}S
v_t	-35mV	-30		

Signal propagation, on the other hand, is characterized using the passive fiber model, as detailed in previous work, which essentially acts as a low pass filter, resulting in decremental conduction throughout the channel and can be mathematically expressed as

$$I_{inTotal} = I_t + I_{out} \tag{4.3}$$

$$I_{inTotal} = \frac{(V_{out} - V_{in})}{R_{lon}} \tag{4.4}$$

$$I_t + C_m\frac{dV_{out}}{dt} + G_L\left(V_{out} - E_L\right) = 0 \tag{4.5}$$

where $I_{inTotal}$ is the net propagating current directed toward the junction/point of measurement, I_t is the transmembrane current due to membrane dynamics, I_{out} is the overall current delivered, V_{in} is the AP generated by the localized

active region, propagating membrane potential at the junction or measurement point, where the initial membrane potential is equal to the resting membrane potential, is denoted by the symbol V_{out}, and C_m is the bulk capacitance for the isopotential compartment, R_{lon} is the axial resistance acting against axial propagation of propagating current, G_L is the leakage conductance due to leakage ion channels in the membrane and E_L is the equilibrium potential of leakage channels. The intersection of the dendritic bifurcation and the 'soma' are taken as a summing node considering Kirchhoff's current law, where current from the two branches propagates and accumulates gradually. Because of the presence of localized AICs near the junctions in terms of an AP, this cumulative current will trigger a combined effect, and the process will repeat itself until the current reaches the 'soma' to trigger the overall response due to the cumulative input stimulus attached to the distal dendritic ends. The distal terminals of neurons are coupled to the inputs in specific patterns, as shown in the connectivity matrix Figure4-7 and Figure4-8. Some of the responses of the simpler neuron morphology shown in Figure4-4a at different locations of localized AICs, namely near the synapses, near the junctions, and at the 'soma' respectively due to different stimulus matrices shown in Figure4-9 are shown in Figure4-10, Figure.4-11, Figure4-12, Figure4-13.

Matrix 1

-45	67	-56
-56	71	-66
-52	69	-78

Matrix 2

67	-56	-45
-56	71	-66
-78	-52	69

Matrix 3

-45	-56	-52
67	71	69
-56	-66	-78

Matrix 4

-45	-56	67
-66	71	-56
69	-52	-78

Figure 4-9: Different orientation 3×3 photoreceptor stimulus matrix connected to the neuron in Figure4-4a via BCs in configuration of vertical edge selective connectivity matrix shown in Figure4-7 to simulate spiking activity at different ion concentrated localized locations of the neuron shown in Figure4-10, Figure4-11, Figure4-12 and Figure4-13.

Figure4-10, Figure4-11, Figure4-12, and Figure4-13 show a variety of fascinating outcomes, beginning with post-inhibitory rebound, post inhibitory bursting, and intrinsic bursting type activity at various sites of the cell. The extreme right panels in Figure4-10, Figure4-11, Figure4-12, and Figure4-13 represent the neuron's overall response, which is then translated to spike rates to quantitatively assess the output response of the layer of neurons. The extreme left matrix 'Matrix 1' in Figure4-9 represents a horizontal gradient fed to a horizontal orientation-sensitive edge configuration, resulting in high regular spiking activity, whereas the same neuron's response to a diagonal gradient results in post inhibitory rebound

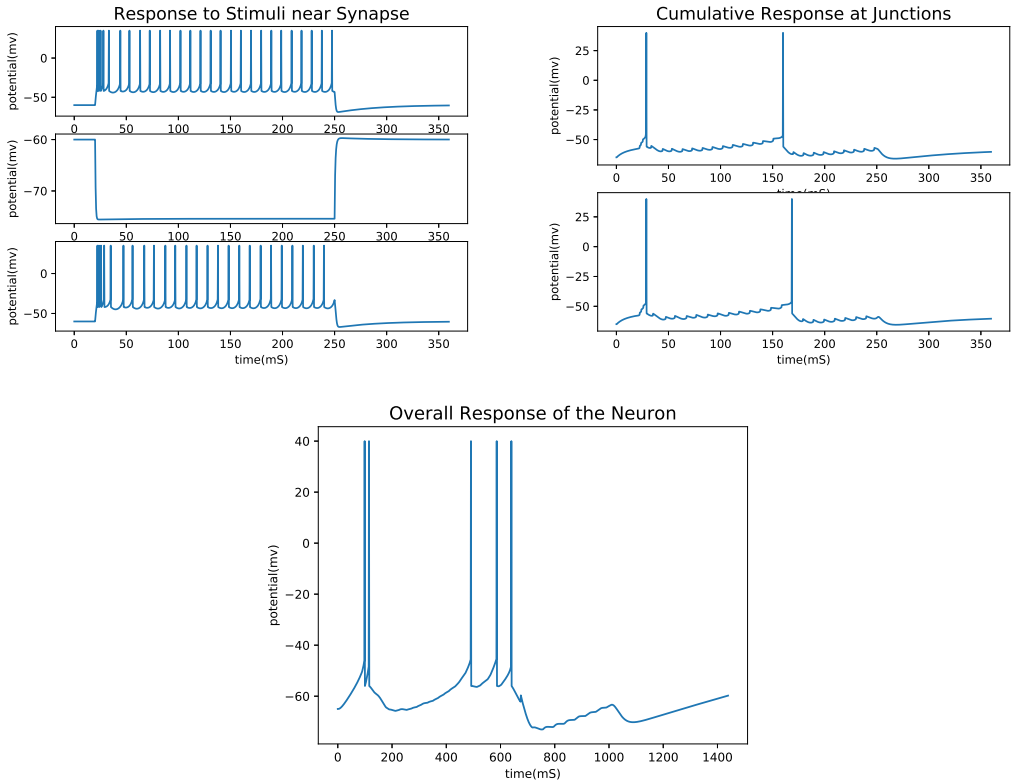

Figure 4-10: Spiking activity due to input matrix 1 near the synapse, at the junctions with localized ion clannels and the soma respectively.

spiking activity with an overall decrease in the number of spikes. The second final test matrix 'Matrix4', which corresponds to a vertical gradient in Figure4-9, however, also leads to post inhibitory spiking activity due to misaligned edge orientation, as demonstrated in realistic OS ganglion cells [210, 211]. The spiking rate is taken into account for encoding and visualizing the response of the modeled neuron network, regardless of regular spiking activity or inhibitory rebound activity, and has been discussed in 4.6.

4.3.3 The Rate Encoder

After the cumulative information in the spatial neighborhood is processed and encoded into a temporal signal in terms of spiking activity by the processing RGC, the firing rate calculator converts the cumulative temporal data back into spatial information. Conversion of temporal to spatial information in the proposed model helps to quantify the response generated and gives a vague perception of probable data projection and representation in a single layer of the V1 neuronal network.

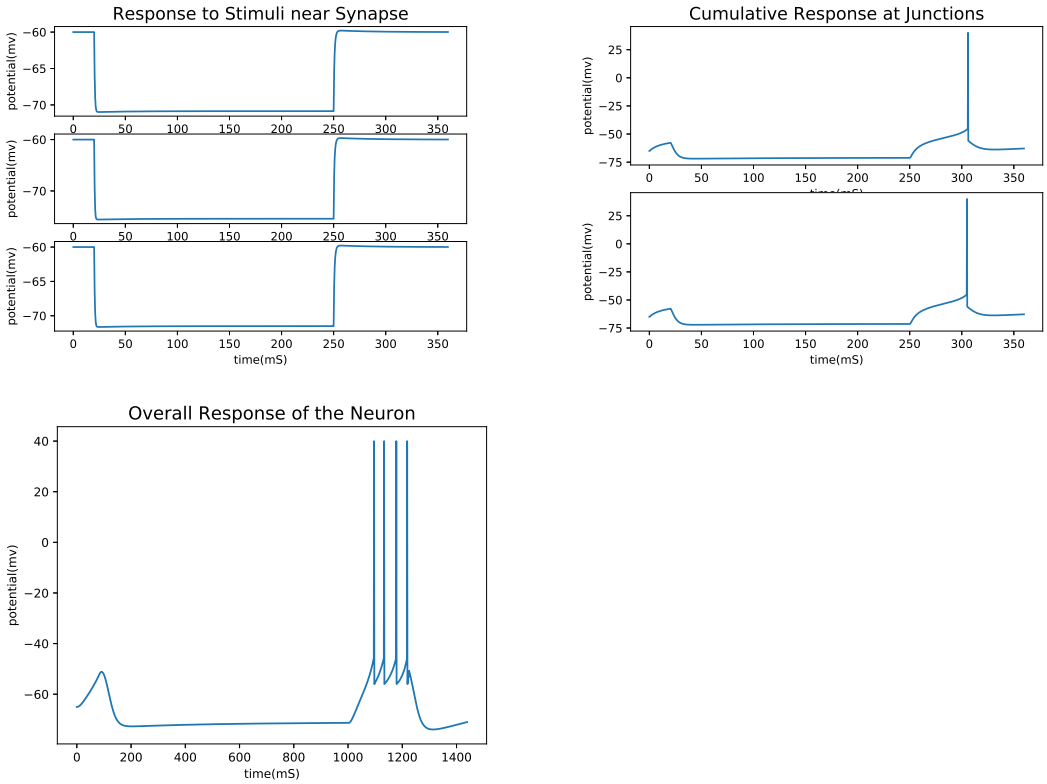

Figure 4-11: Spiking activity due to input Matrix 2 near the synapse, at the junctions with localized ion clannels and the soma respectively.

Quantification of the temporal data back to spatial information is done using

$$F_x(i,j) = \frac{\sum_{k=0}^{n-1} F_x(i,j) + 1|_{V_{m(i,j)}(t) > V_{threshold}}}{t} \tag{4.6}$$

where $i,\ j$ represents the localized neuron, $V_{m(i,j)}\,(t)$ represents the temporal voltage response of the neuron cell body, $V_{threshold}$ is the minimum membrane potential for a spike to trigger and t is the total time duration of the temporal response. $F_x(i,j)$ is the localized spatial information and gives the spiking rate of particular localized cell of interest in terms of $spikes/sec$. Total spatial information represents the overall response of the single layer of neuron.

4.4 Orientation Selectivity & Edge Map Extraction

The process of Orientation Selective feature extraction has been explored in the human visual cortex in terms of scotopic and color vision. The scotopic vision configuration is like color vision except for gray-scale and RGB image input. Figure

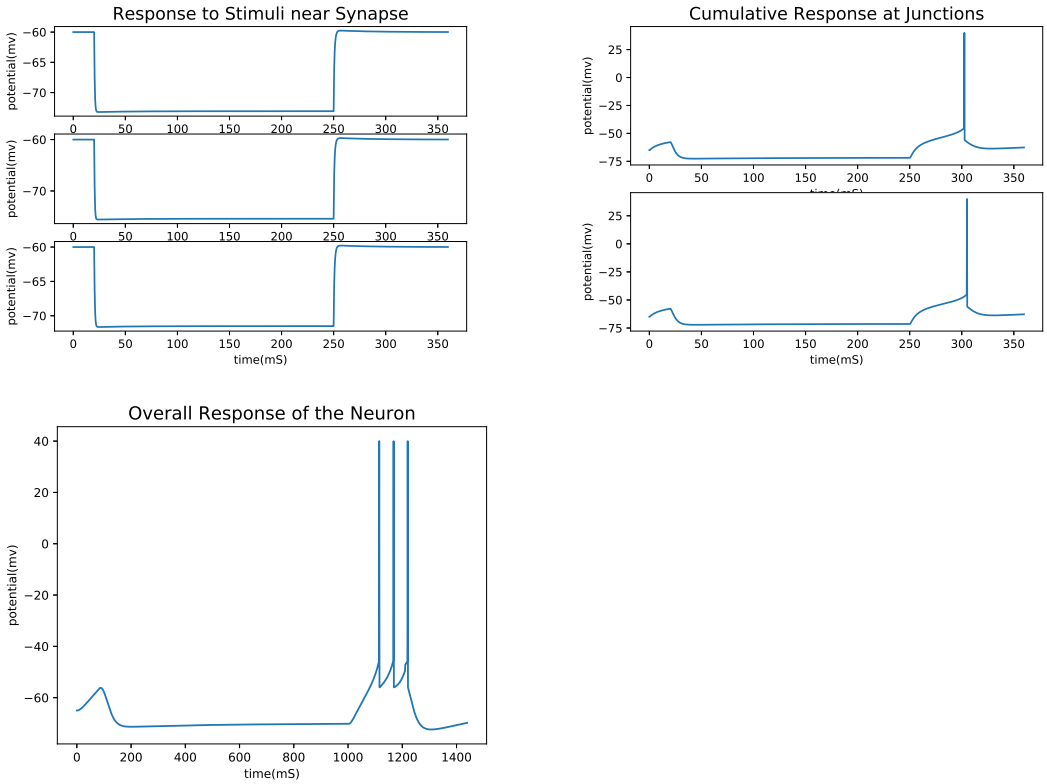

Figure 4-12: Spiking activity due to input Matrix 3 near the synapse, at the junctions with localized ion clannels and the soma respectively.

4-15a depicts a sample input patch supplied to the model for a better understanding of the model dynamics. Corresponding responses for 0° and 90° selective RGC cell are shown Figure4-15b and Figure4-15c respectively. The figures clearly illustrate the local responses at distal dendrites, junctions, and soma. The RGC starts resonating at high frequencies when the input patch matches the preferred Orientation. The spiking frequency of the RGC significantly decreases on getting stimulation with non-preferred orientation [187, 212–214].

Similar responses for preferred and non-preferred activity are mimicked by the designed Orientation Selective RGC in Figure4-15b and Figure4-15c. The Orientation Selective RGC performance has been verified with multiple oriented feature neighborhoods. The consistent behavior of RGC has been obtained for preferred as well as non-preferred orientations as reported in the literature.

Natural test images are fed as input to the proposed model, and population responses of identical Orientation Selective modular RGC are collected. The RGC population layer with particular Orientation Selectivity is responsible for the extraction of preferred orientation features. Multiple stacks of oriented feature maps are obtained by configuring the RGC population at 0°, 45°, 90° and 135° specificity

Table 4.2: Orientation selective ON RGC layer response at 0°, 45°, 90° and 135° orientation and OFF RGC layer response at 0°, 45°, 90° and 135° orientation in scotopic vision corresponding to sample images in Figure4-16a.

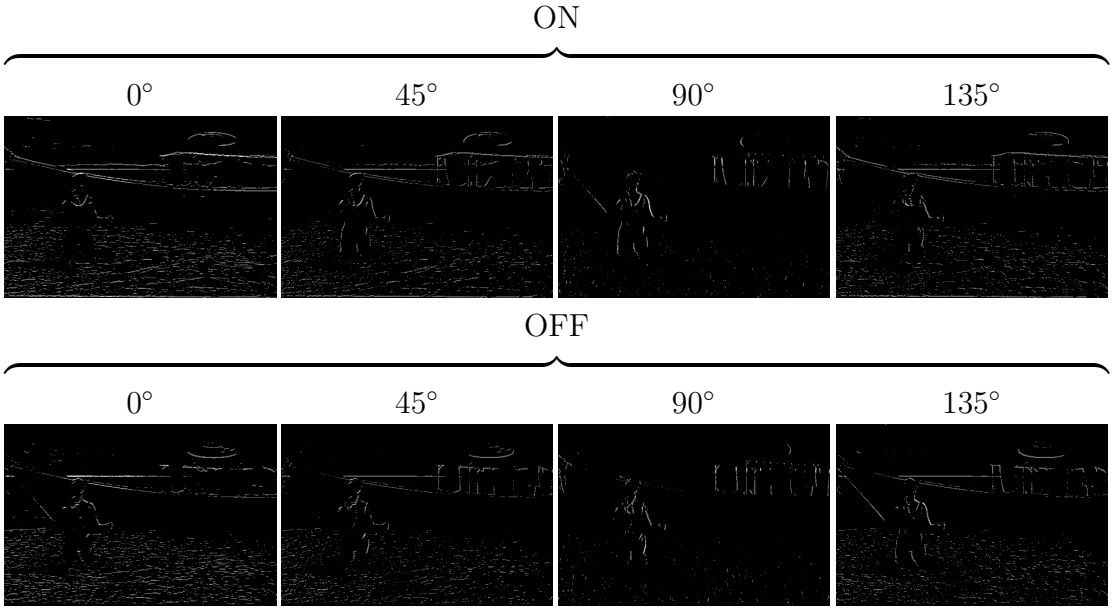

Table 4.3: Orientation selective ON RGC layer response at 0°, 45°, 90° and 135° orientation and OFF RGC layer response at 0°, 45°, 90° and 135° orientation in scotopic vision corresponding to sample images in Figure4-16b.

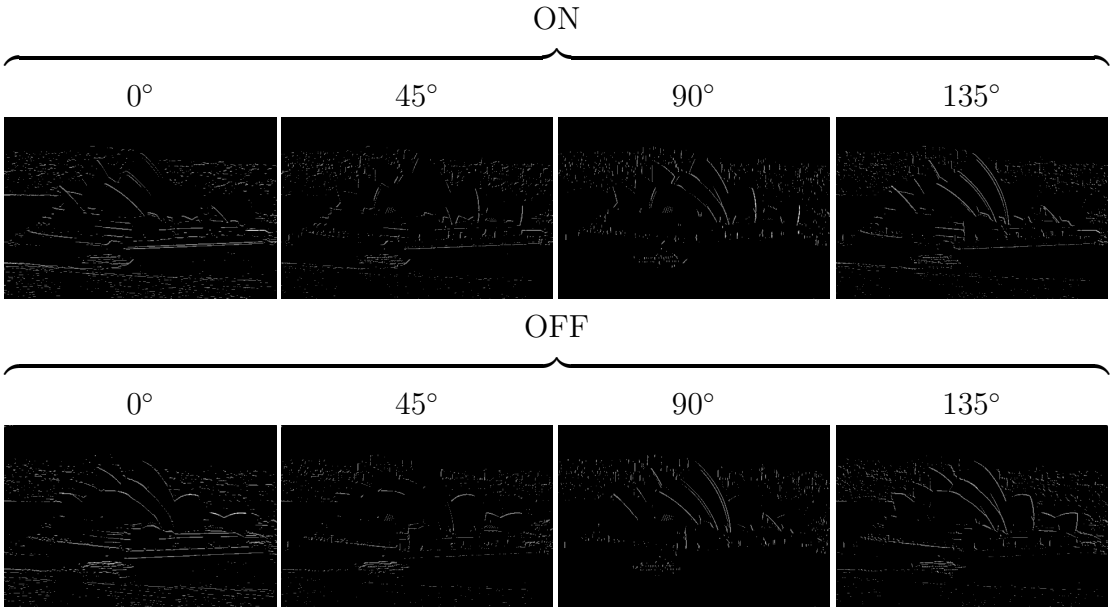

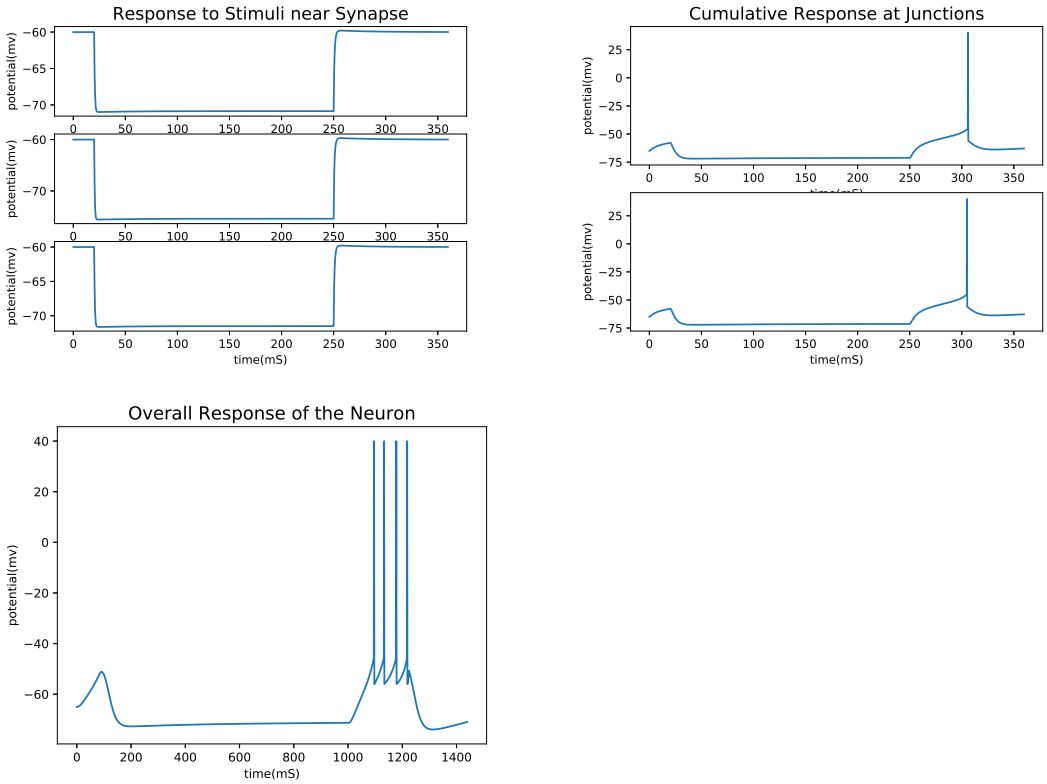

Figure 4-13: Spiking activity due to input Matrix 4 near the synapse, at the junctions with localized ion clannels and the soma respectively.

with ON and OFF phases. The obtained Orientation Selective RGC responses for ON and OFF phases of Figure4-16a and Figure4-16b are shown in Table. 4.2 and Table. 4.3 respectively. The complete edge-map responses in Figure. 4-17 are computed by max-pooling of different Orientation Selective RGC layers. The orientation responses for the scotopic vision are computed with the gray-scale image, whereas the 'red,' 'green,' and 'blue' channels are utilized for color vision. Four ON phase Orientation Selective and four OFF phase Orientation Selective RGC layers are dedicated for scotopic vision. Similar operations are performed in color vision individually on the three layers for Orientation Selectivity, and the final edge-map is generated. Figure 16 are the scotopic population responses of Orientation selective ON and OFF RGC network layers with orientation specificity of 0°, 45°, 90° and 135° respectively. The spiking frequency is used to quantify the temporal responses into spatial feature space using equation 4.6.

Shown in Table.4.2 and Table.4.3 are the scotopic population response of OS ON and OFF RGC network layers with orientation specificity of 0°, 45°, 90° and 135° respectively in terms of spiking frequency and shown in Figure4-17 are the complete edge-map generated by max-pooling from the ON and OFF RGC population responses.

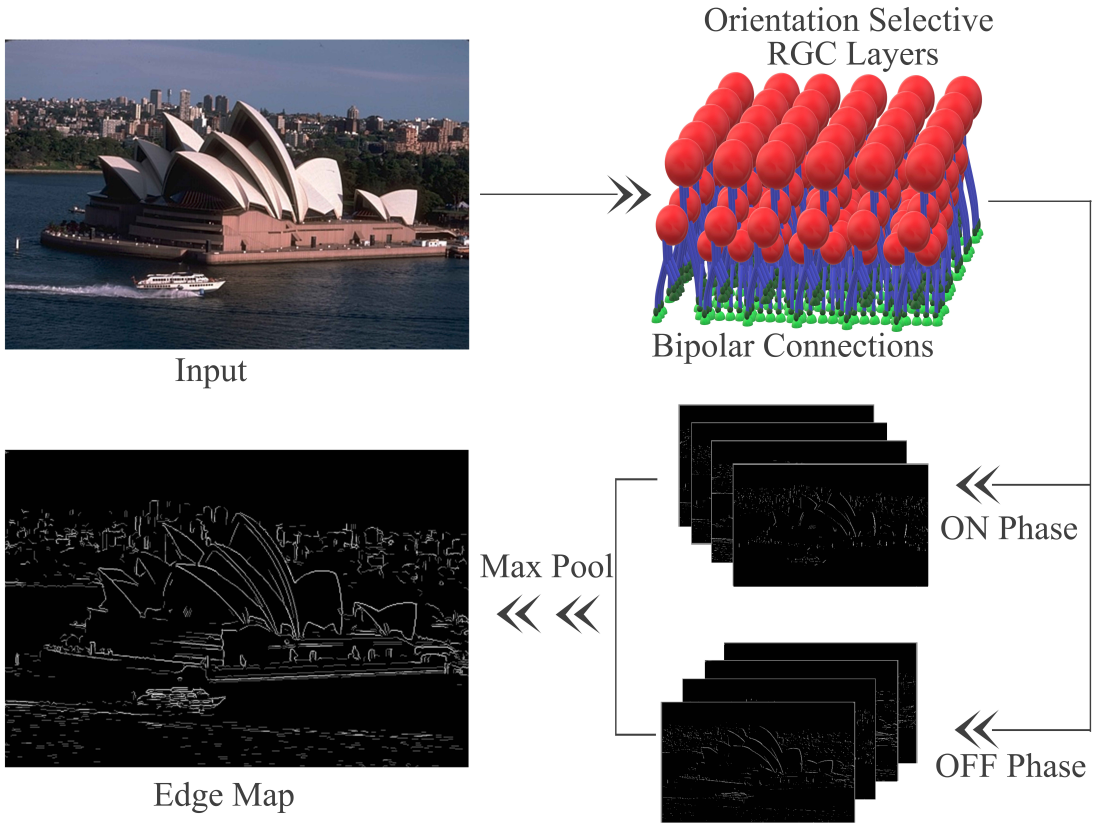

Figure 4-14: BC (ON in light green and OFF in dark green semi-sphear) connetivity of orientation selective RGC in human primary visual cortex showing oriented feature extraction and edge estimation.

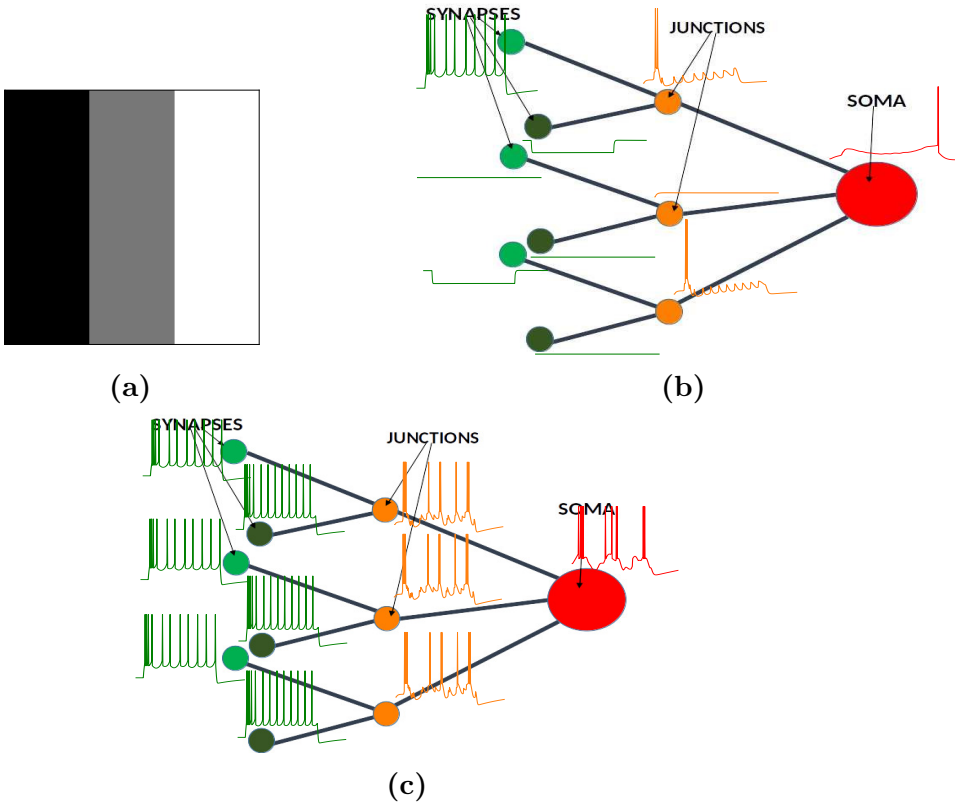

Figure 4-15: RFs connectome specificity for RGC in Figure4-4 cell connectivity. **(a)** Sample vertical gradient input patch to 0° and 90° Orientation Selective RGC cells, **(b)** Response at different locations of the 0° Orientation Selective RGC cell corresponding to the input sample data shown in Figure4-15a fed to the photoreceptor cell, and **(c)** Response at different locations of the 90° Orientation Selective RGC cell corresponding to the input sample data shown in Figure4-15a fed to the photoreceptor cell.

(a) Sample image 81066.jpg **(b)** Sample image 69000.jpg

Figure 4-16: Sample input image from BSDS database for ON and OFF RGC oriented edges.

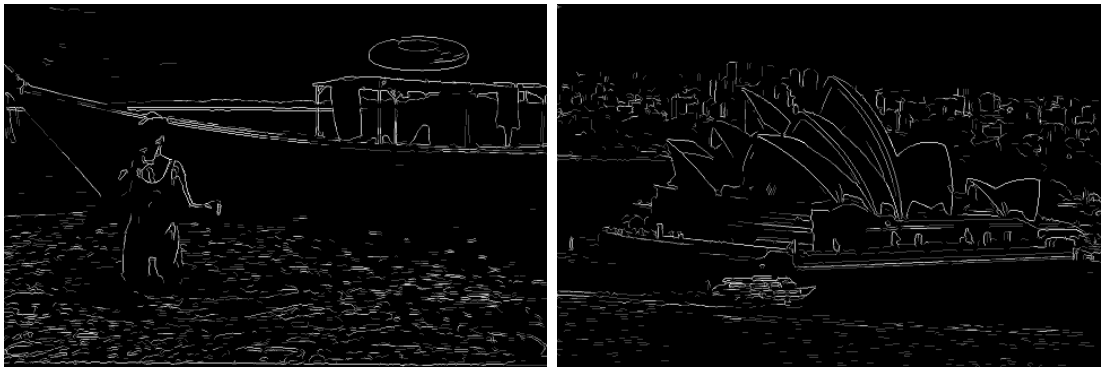

(a) Sample edge map for image in Figure. 4-16a

(b) Sample edge map for image in Figure4-16b

Figure 4-17: Sample edge reconstructed images from ON and OFF RGC oriented edges (scotopic vision) for the sample images in Figure4-16.

4.4.1 Simulation Results for Scotopic & Color Vision

The proposed model has been simulated using 'Python 3.6' interpreter. The 'open CV' and 'scikit' packages are exploited for basic image operations, and differential equations are solved using 'scipy.integrate'.

The selected parameters to implement Izhekivich's membrane dynamics and passive signal propagation are presented in Table 4.1. The inputs to the obtained model are images in 'tif,' 'png' and 'jpg' format. These inputs have been collected from the Berkley segmentation database (BSDS500) [215]. Nearly sixty inputs are fed to the proposed model, but the responses corresponding to six typical input images are presented in this work. The selected image dataset that comes with edge ground truth is considered as a reference for performance estimation using 'Piotr's Matlab Toolbox' [216]. The photoreceptor receiving natural images as stimulus yields Orientation Selective maps. The final edge map estimation is obtained using Maxpool operation on four Selective Orientation maps of two different phases as shown in Figure4-18. The 'matplotlib' package has been used for the plotting of image responses and cell dynamics temporal signals. The 'Scotopic edge' and 'Color edge' responses of Figure4-18 incorporate the scotopic and color vision model of the human primary visual cortex. The presented model successfully mimics the behavior of RGC responses to rod and cone inputs. The RGC response to cone cell input maps the relative spectral component along with the rate of absorption, whereas the rod cell fails to map the relative spectral components. A careful visual comparison of 'Color' and 'Scotopic edge' responses corresponding to Figure4-18(a) input reveals the relative spectra discrimination capability of cone cells. The color vision response successfully detects the contour

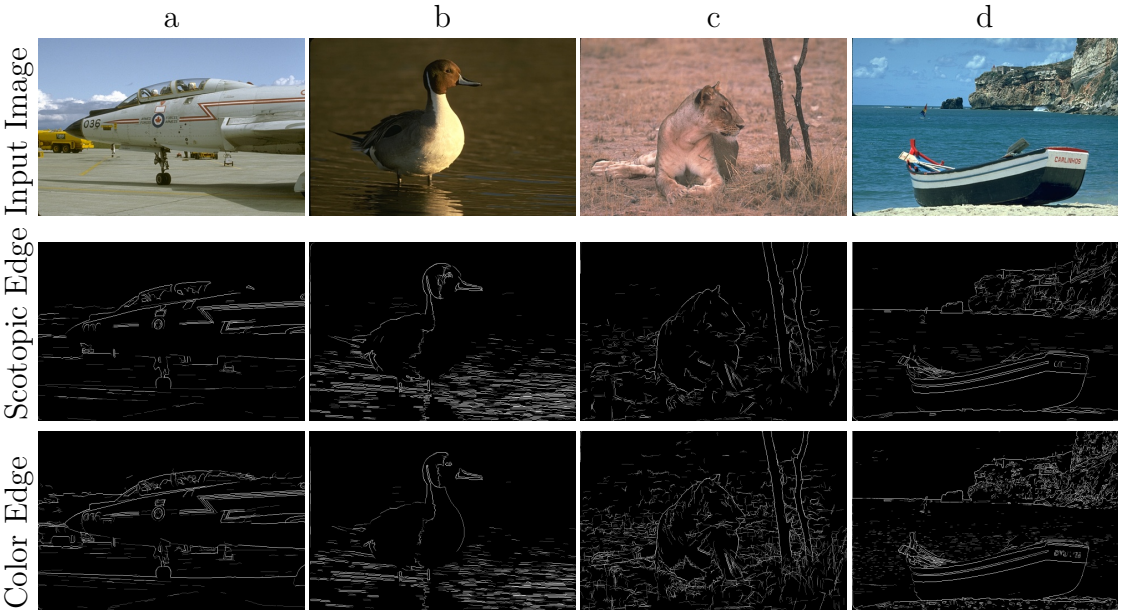

Figure 4-18: Edge detection response of the scotopic vision model and color vision model to some input images

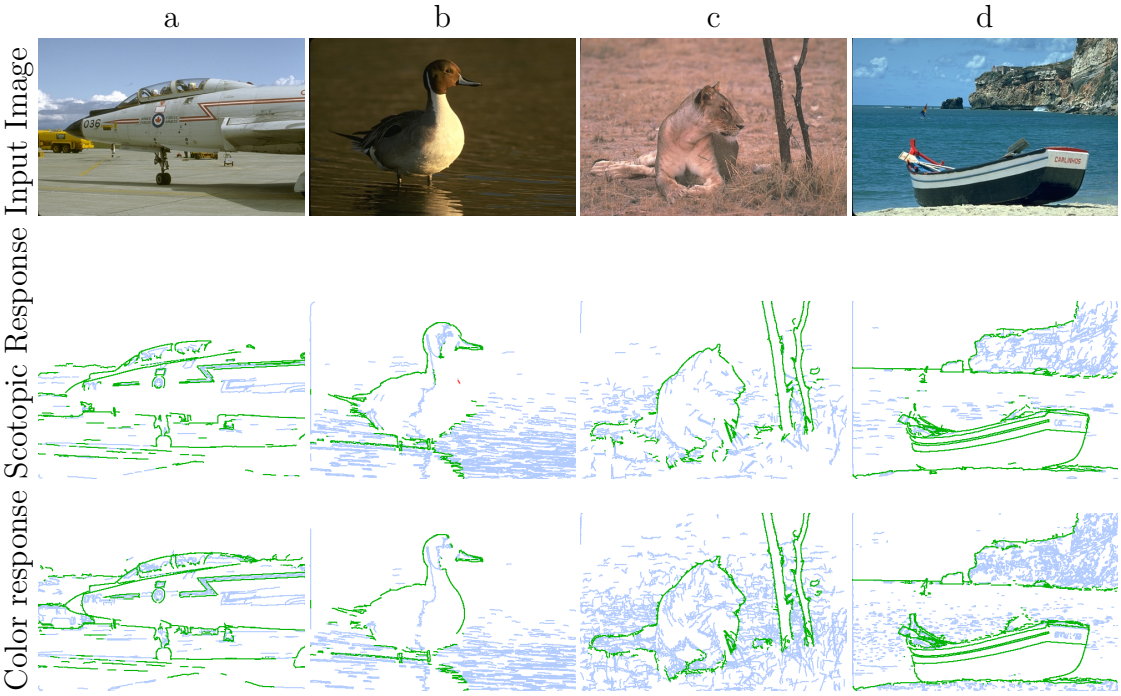

Figure 4-19: Visualizations of matches and errors of scotopic vision and color vision compared to BSDS ground truth edges. Edges are thickened to two pixels for better visibility; the color coding is green=true positive, blue=false positive, red=false negative.

between the aeroplane and sky, whereas the scotopic vision fails to map the relative change in spectral component. The rod inputs to the RGC cell successfully map the rate of absorption that enables night vision [217]. But the homogeneity of absorption at the contour made the scotopic vision fails to detect the edge gradient. Similar responses are visible corresponding to the Figure4-18(b) input as well. The scotopic vision tracks the darker edges and textures in Figure4-18(b) near the beak and wings, whereas color vision fails.

The accuracy of the model is further assessed by match and error of responses. The visualization of edge match and errors of scotopic and color vision model is shown in Fig 4-19. The blue and red edges indicate false-positive and false-negative edges, respectively. The green edges confirm the matching of the ground truth edge with the model detected edge. The performance of the proposed modelled is effectively demonstrated by comparing it with existing state-of-the-art neural-network model [218–225]. The selected performance parameters are OIS and ODS. The response of the proposed model shows a good true positive profile and false-negative profile compared to the state-of-the-art model [223]. The models reported in [218, 220–222] are compared with the proposed model. The compared performance parameters are presented in Table 4.4. The proposed model successfully mimics human visual perception and capability, although its performance is comparable. To create the edge picture from an edge probability map, a threshold is required. To set this threshold, there are two options. The first method, known as optimal dataset scale (ODS), uses a constant threshold over the whole dataset of photographs. The second method, known as optimal image scale (OIS), chooses the best threshold from Richer Convolutional Features for Edge Detection for each image [226]. The OIS scores obtained through the model reach the human edge perception reference of 80% [218, 219]. However, the decline in the optimal image scale F-score ODSF and optimal dataset scale F-score OISF scores is due to more number of false positives and its inability to suppress non-maxima.

The low performance of the model in terms of false-positive is due to the size of the used RF. The small RF midget RGC identifies even the fine textures as edges. These edge maps, along with fine textures, when fed to the 'Piotr's Matlab Toolbox' [216] result in compensated OISF and ODSF scores. This can be minimized by incorporating parasol cells with a larger RF. Successful suppression of non-maxima can be achieved with large RFs. But the proposed work is limited to midget RGCs.

Table 4.4: Performance comparison of the proposed framework with existing state-of-the-art-models on BSDS500 database

Reference	Methods	ODS	OIS
[218]	RCF	0.806	0.823
[221]	DeepContour	0.757	0.776
[219]	Human	0.803	0.803
[219]	BDCN	0.779	0.792
[219]	BDCN-w/o SEM	0.778	0.791
[220]	DeepEdge	0.753	0.772
[222]	HED	0.788	0.808
[223]	SE	0.75	0.77
[224]	Multicue	0.72	-
[225]	CEDN	0.788	0.804
This work	**Scotopic Vision**	**0.717**	**0.771**
This work	**Color Vision**	**0.668**	**0.815**

4.5 Coupled Orientation Selectivity & Bandwidth Tuning

With the introduction of techniques like EEG, MEG, fMRI, [158–160], capable of capturing local activities in the brain, neuronal electric local potential has been explored in depth and suspected to play a vital role in mapping and researching neural network activity. Over the past few decades, research on LFPs and cell-field interactions has successfully connected LFPs to phenomena [161, 162] that are connected to APs' causal function. LFPs can be attributable to activities and interactions within a constellation of synapses induced by the mobility of neurotransmitters or ionic disturbances caused by the generated electric field accompanied by signal transmission in bundled nerve fibers. The presented work explores the influence of mutual interaction caused by induced electric fields of propagating signals in a system of bundled neural fibers, in addition to synaptic interactions. Because they are the results of transmembrane currents [164, 165] and the induced electric field [168] caused by neuronal activity, and because they highly correlate with associative network dynamics relating to more complex functional responses [166, 167], such as cognition, memory, motor control, theories relating to LFPs due to local neuronal fiber dynamics are widely accepted [163]. Neuron models, such as in [227], discuss the impacts of transmembrane current and cell-field interaction [168], which had previously been overlooked and has significant implications in terms of local dynamics, whilst software models, such as ELFENN in [169], were also developed to mimic the ephaptic effects.

The complexity lies in understanding the spatial spread of cell-field interaction, in addition to the effects and applicability of LFPs. Recent understanding of the process defines the effects as generally local within a range of $200 - 400\mu m$ [228, 229], whereas earlier literature describes the spread of LFPs as both lateral and vertical and ranges from $600\mu m$ to $5mm$ [230–232]. When investigating the vertical spread of LPF, high coherence correlations are found [233], but another literature [234] discusses it as a probable cause due to volume conduction. According to researches conducted in the auditory cortex (A1) [235] and the retinal surface (V1) [228, 229], there is accurate and consistent mapping of sensory receptors that enables LFPs to spread not only spatially but also vertically. Looking more closely at the relationship between LFPs and transmembrane current as communicated in [164, 165], active membrane directly influences transmembrane current caused by rapid inflow/outflow of ions, which affects the local charge density, which in turn influences the local field potential. Aside from the active membrane, the ectoplasmic conductance, which acts as a current sink, also has a significant influence on the strength of the local field potential. Relatively low ectoplasmic conductance results in enhanced LFPs and vice versa, which is most likely due to its current sink characteristics, [236]. Experiments on squid giant axon [173], crab motorneuron [174], frog sciatic nerve [176], and algal strand [175] revealed that stimulating a single fiber from a bundle of nerve fibers could depolarize other fibers caused by the effects of transmembrane current and ionic perturbation within the proximity. Studies [177, 178] discuss in-field DC shift, theta oscillations, phase precision firing, and reciprocal excitability effects due to LFPs in similar experimental studies focused on grid cells and ganglion cells, respectively. Another literature [237], primarily focused on the mammalian olfactory system highlights axon interaction as relatively insignificant due to the presence of thick myelin, which provides electrical isolation, and relatively large extracellular space, which provides quick dispersion of transmembrane current with negligible field potential. Neurons in the mammalian olfactory system lack myelin and could be a crucial predictor of olfactory codes. Innumerable pieces of literature recommend that ephaptic coupling of neuronal fibers could be fundamental and plays a very important role in the stabilization of such a robust, complex system, [238–240], ensuring effective information processing and transmission with negligible error. The richness of ephaptic interactions draws our attention toward a careful assessment of the mechanisms involved in transmembrane current and cell-field interactions. The proposed work incorporates the effects of transmembrane current, cell-field interaction, and morphologically dependent electrical attributes into the cable model and is relatively simple compared to the existing state-of-the-art models discussed in [168, 169, 227, 239, 241–243]. A (passive) compartmental cable equivalent neu-

ron approach has been implemented to mathematically model the transmission of signals and the effects of transmembrane current in a bundled fiber system devoid of myelin sheath [237], as well as its overall effects on local field potential and inter-fiber interference while accounting for inter-cellular and intra-cellular cytoplasmic in-homogeneity. On the contrary, if the local attributes corresponding to the localized region (geometric as well as electrical properties) are known in advance, such a model can be easily extended to study the effects of local field potential in bundled fiber systems as well as complex neuronal networks. The proposed simulation is performed using biological parameters from [244–247] and the geometrical dependence of the coupling parameters is inspired by works from [168, 170–172, 237].

4.5.1 Implemenation of fiber coupling in primary visual cortex

The proposed coupling model has been implemented in detail in a single layer of primates' visual cortex models discussed in Section 4.3. RGC with six dendritic inputs with connectome specificity inspired by 'Sobel filter' controlling the orientation selectivity, dendritic spread controlling the spatial scale, and the neuron's bandwidth is controlled by a combination of active membrane dynamics due to localized AIC. Each of the input distal dendrites has been connected to a bipolar cell RF, Figure4-6, that is in turn connected to photo-receptor cells, thereby transducing the light stimuli trapped by the photoreceptor cells and converting them into Spatio-temporal signals, Figure4-2 and Figure4-3. Detailed organization and architecture of the PVC are shown in Figure4-4b. Spiking activity due to localized active membrane dynamics has been modeled using the Izhekivich 'bursting' and 'chattering' type spiking activity, and propagation parameters are taken and shown in Table.4.1. Input to the coupled model is 'tiff,' 'png' or 'jpg' image files which are converted to Spatio-temporal square pulse signals of 200 $mSec$ with an offset of 10 $mSec$ and pulse width of 150 $mSec$. Dendritic spread of the modeled system of RGC takes Spatio-temporal signal within a grid size of 3×3 BCs and connectome specificity shown in Figure4-8. Modeling inter-fiber coupling arrangement is as shown in Figure4-20 with coupling matrix for fiber n_7 with a 3×3 BCs neighbor is shown in Table.4.6. As shown in Figure4-20, for a connectivity matrix within a 3×3 BCs neighborhood surrounding information in n_{13} (in right bottom corner), dependent fiber connections of the RGC are n_7, n_{12}, and n_{17} with ON-BC whereas connectivity n_9, n_{14}, and n_{19} are corresponding to connectivity with OFF-BCs. In order to simulate the fiber dynamics in fiber connected to n_7,

the coupled model takes a neighborhood of 3×3 grid surrounding the fiber of interest n_7 (in right top corner), where mutual coupling parameter dependence for the connectivity n_1, n_2, n_3, n_6, n_7, n_8, n_{11}, n_{12} and n_{13} are as shown in Table.4.6. To simulate the effects of the coupling matrix shown in Table.4.6, similar coupling computations are performed in individual fibers, and the cumulative response for the RGC neuron of interest has been computed for each spatial location of the natural scene fed as input to the layer of RGC neurons.

4.5.2 RGC Dendritic Input Coupling:

RGC coupling and its effects on neuronal computation are still unknown, and the field has been unexplored due to the computational complexity of the system of coupled equations. In this work, an attempt has been made to integrate bundled fiber coupling to better understand the role of neuron fiber coupling in neuronal computations. While computing the cumulative response of morphologically detailed RGCs with localized AICs, a neighborhood of 3×3 BC neighborhood has been considered where the connectome specificity of the RGC is dependent on the connectivity matrix shown in Figure4-8.

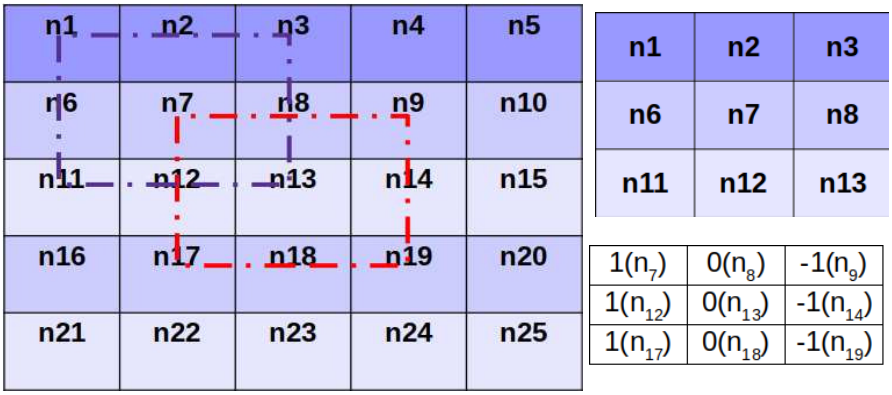

Figure 4-20: Coupled fiber connectivity neighborhood (top right) concerning central fiber of interest at n_7 for connectome specificity for detection of verticle edges shown in connectivity matrix(bottom right) superimposed over the red block for computing overall orientation response at n_{13}.

Apart from connectome specificity, for computation of coupled bundled fiber system an example neighborhood is shown in Figure4-20, where a 5×5 BC neighborhood has been considered to compute the response of the OS-RGC at n_{13} and a 3×3 neighborhood is represented with the 'box in red' in Figure4-20 which suggests inputs connected to n_7, n_{12}, n_{17} and n_9, n_{14}, n_{19} configured for vertical edge selectivity. At each location of these inputs, coupled responses are computed.

If the coupled response of input dendrite connected to BC n_7 is considered, a 3×3 BC neighborhood has been considered for the coupled input response in dendritic input at n_7, represented with the 'black box' surrounding n_7 top right corner of Figure4-20 and depending on temporal dynamics at the surrounding fibers, the coupled response at the central fiber is computed using equation (3.43) and discussed in details in Section 3.4.1. The corresponding coupling parameter between the 9 fibers within the neighborhood of n_7 is coupled with coupling parameters given in Table.4.6. Similarly, coupled responses for every dendritic input for the RGC are computed.

A positively coupled system in the coupled model suggests that the neighboring fiber contributes positively to the central BC fiber proportional to the amount of depolarization or hyperpolarization experienced in the nearby fibers, and the overall response of the central fiber is a dependent temporal response corresponding to the central BC intensity along with a weighted sum of the neighboring cell responses. Under such configuration, similar spatial information in the neighborhood results in an amplified overall response in the central fiber, whereas dissimilar information within the neighborhood results in a proportionately suppressed response in the central fiber. Such an approach has been adopted to compute the overall response of individual RGC cells to replicate the orientation-selectivity behavior of the RGC network and compared against a histogram of oriented gradients(HOG) features to analyze the accuracy of orientation selectivity of the proposed model with the uncoupled counterpart.

HOG feature extraction and comparison with the orientation selectivity shows the degree of accuracy of the proposed orientation selectivity scheme. HOG is a feature descriptor that is used in computer vision and image processing to recognize objects. The technique counts the number of times a gradient orientation appears in a limited region of an image which is comparable to edge orientation histograms, scale-invariant feature transform descriptors, and shape contexts but computed on a dense grid of evenly spaced cells and employs overlapping local contrast normalization for increased accuracy. The core idea behind the HOG descriptor is that the distribution of intensity gradients or edge directions can be used to characterize the appearance and shape of local objects within an image.

4.5.3 Orienation Selectivity Bandwidth Representation

Figure4-21 shows a sample image from BSDS [215] image database used in the proposed uncoupled model for OS edge detection and histogram bandwidth rep-

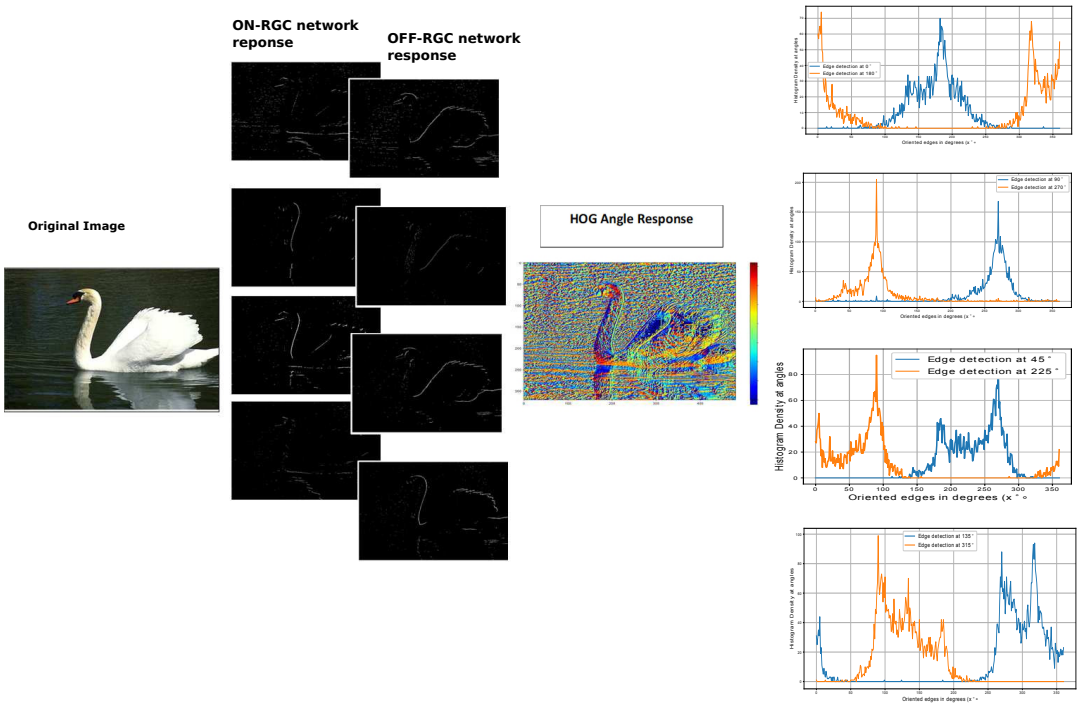

Figure 4-21: Sample process of detection of uncoupled OS edge extraction in an image from BSDS database and convoluting with the HOG angle image to extract histogram of extracted edge orientation angles.

resentation for orientation-selectivity. The sample image has been fed to the OS ON-BC RGC network and OFF-BC RGC network to compute OS edge information at 0°/180°, 45°/225°, 90°/270° and 135°/315° as shown. Along with the OS edge information, HOG angles of the gradient have been computed, and the color bar near the HOG angle response shows the ranges of gradient angles captured by the HOG feature extractor that ranges from 0° to 359.99°. This gradient angle information from the HOG angle response is convoluted with the binary OS edge responses of the ON and OFF RGC network to acquire information about gradient angle information at the precise OS edge regions to visualize the bandwidth of orientation-selectivity of the uncoupled network of RGC as shown in the extreme right plots in Figure4-21. A similar process has been repeated to construct the orientation-selectivity in the case of the coupled RGC network and compare the bandwidth tuning in the coupled network.

4.5.4 Simulation Results

The proposed model has been simulated using ‘Python 3.6’ interpreter. The ‘open CV’ and ‘scikit’ packages are exploited for basic image operations, and differential equations are solved using ‘scipy.integrate’.

The parameter in Table.4.5 r_a, r_e are the intracellular and extracellular resistance of cytoplasm, whereas c_m, r_{leak} are membrane capacitance and membrane leakage resistances respectively. The intracellular cytoplasmic resistance is considered higher as compared to the extracellular counterpart[168, 170] considering low ionic mobility due to confined space inside the neuronal fiber and higher ionic mobility in extracellular space. Apart from the mobility of ions, conduction in extracellular as well as intracellular cytoplasm takes place due to volume conduction, whereas the membrane parameters such as membrane capacitances and membrane resistances contribute due to surface diffusion or accumulation of ions. Cell-field interaction due to signal propagation in nearby fiber reorganizes ionic distribution and membrane potential dynamics of the nearby fiber[168, 170]. The induced field is spherical, with the strength of the field decreasing radially outward. Interaction of electric field with other fiber takes place due to electrically-induced transmembrane current and is dependent on morphological as well as electrical attributes of neuronal cell[168, 170]. Morphological consideration such as size, shape, the Orientation of fiber concerning the induced electric field, and inter-fiber spacing has been taken into consideration while computing coupling parameters, whereas electrical properties such as membrane leakage resistances and membrane capacitances are taken from [2, 3, 205].

Table 4.5: Neuron attributes considered for generation of coupling matrices.

r_a	r_e	c_m	r_{leak}
$166\Omega - cm$	$63\Omega - cm$	$1\mu F/cm^2$	$40K\Omega - cm^2$
volume conduction	volume conduction	surface conduction	surface conduction
$\frac{4r_a l}{\pi D^2}$	$\frac{4r_e l_{xy}}{\pi D_{xy}^2}$	$c_m \pi D l$	$\frac{r_{leak}}{\pi D l}$

To replicate similar coupled bundled fiber behavior in an RGC network, a 3×3 bipolar neighborhood has been considered. For a 3×3 BC connectivity neighborhood arrangement shown in Figure4-20, inter-fiber coupling parameters are calculated and designed as shown in Table.4.6 such that the fiber bundle associated with the central BC of 3×3 neighborhood is positively coupled corresponding to the neighboring fibers. In the Table.4.6, the row and column names n_x corresponds to fiber-x and the value corresponding to the n_x row and n_y column is the inter-fiber resistance between the fiber-x and fiber-y. For n_x row and n_y column with $x = y$ corresponds to the axial resistance of the fiber-x (diagonal components of the Table.4.6 with value 15).

In the proposed work, to compute the orientation selectivity efficacy, HOG features from the original image have been computed along with the OS response

Table 4.6: Coupling matrix for the coupled fiber system considered for fiber coupling neighborhood with respect to the fiber of interest at n_7.

	n_1	n_2	n_3	n_6	n_7	n_8	n_{11}	n_{12}	n_{13}
n_1	15	20	0	20	3	0	0	0	0
n_2	20	15	20	20	3	20	0	0	0
n_3	0	20	15	0	3	20	0	0	0
n_6	20	20	0	15	3	0	9	9	0
n_7	18	18	18	18	15	18	18	18	18
n_8	0	20	20	0	3	15	0	20	20
n_{11}	0	0	0	20	3	20	20	15	0
n_{12}	0	0	0	20	3	20	20	15	20
n_{13}	0	0	0	0	3	20	0	20	15

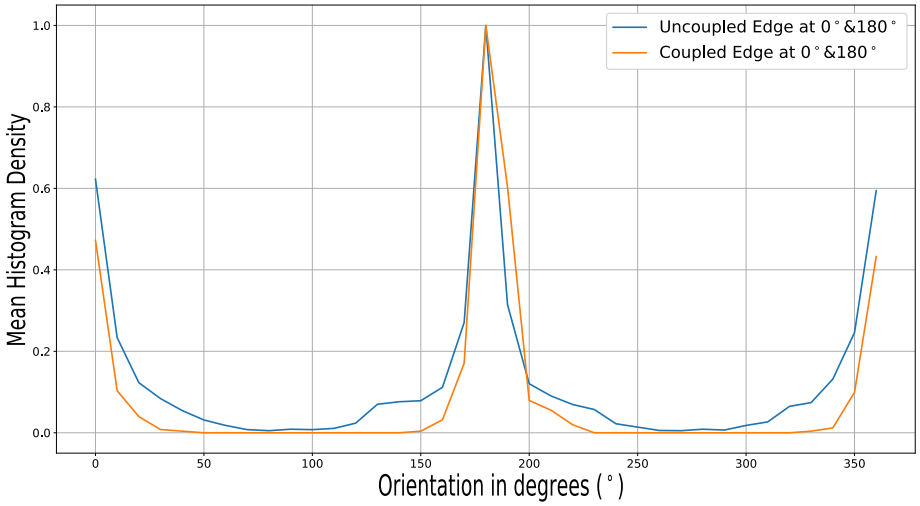

Figure 4-22: Normalized histogram selectivity of the coupled RGC network and uncoupled RGC network computed at 0°/180° from test images.

of the RGC model. Pixel-wises multiplication of the HOG features and OS responses are computed to find the edge orientation information of the detected oriented edges. Similar computations are made to extract edge orientation information extracted by the coupled RGC layer as well as the uncoupled RGC network layer and represented in terms of a histogram of edge orientations. When comparing the HOG feature in a coupled RGC network to its uncoupled counterpart in Figure4-22, Figure4-23, Figure4-24 and Figure4-25, the coupled network shows lower histogram density with edge orientation detection band tuned to preferred orientation, which is attributable to enhanced selectivity to orientation information. Comparing the histogram density spread of the coupled RGC network to the uncoupled counterpart, the spread appears to concentrate within an orientation selectivity range of ±45° in the coupled system, whereas the uncoupled counter-

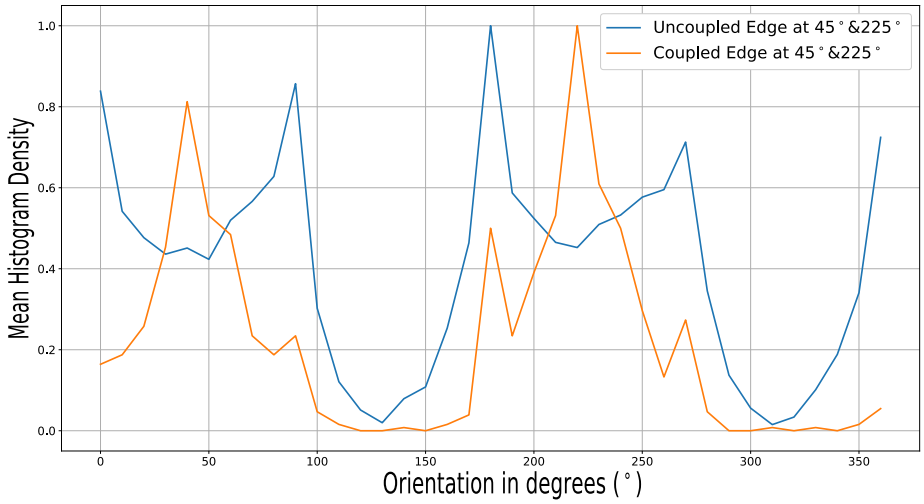

Figure 4-23: Normalized histogram selectivity of the coupled RGC network and uncoupled RGC network computed at 45°/225° from test images.

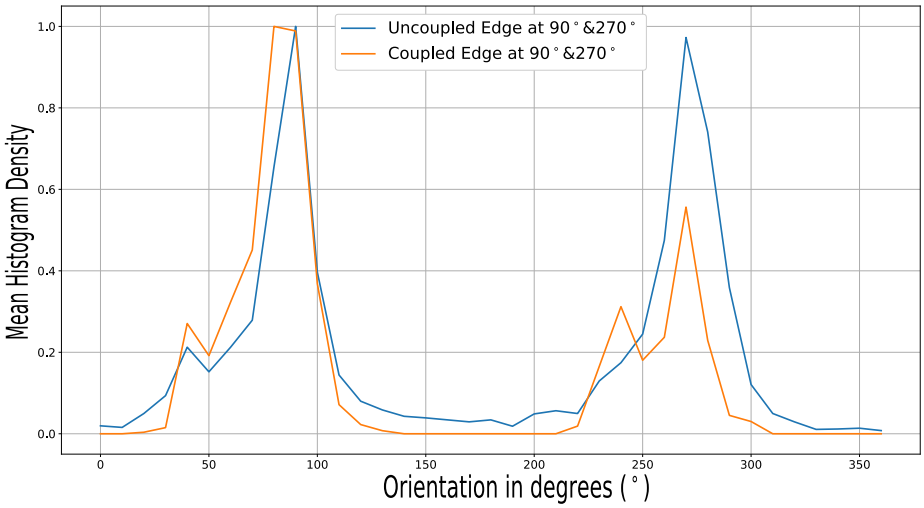

Figure 4-24: Normalized histogram selectivity of the coupled RGC network and uncoupled RGC network computed at 90°/270° from test images.

part has an orientation selectivity range of ±90° which might further be improved with appropriate coupling parameter corresponding to orientation selectivity. The model has been tested and analyzed using the Berkeley Segmentation Data Set 500 (BSDS500)[215] and found consistent in terms of edge orientation tuning and edge detectability.

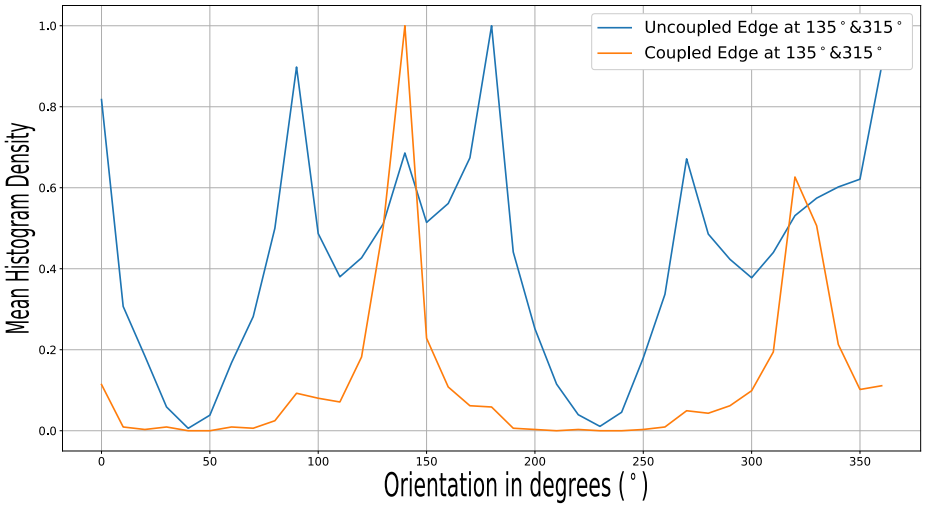

Figure 4-25: Normalized histogram selectivity of the coupled RGC network and uncoupled RGC network computed at 135°/315° from test images.

4.6 Summary and Future Remarks

This chapter bridges the gap between the dynamics of local neuron morphology and global responses. The presented model successfully linked the human visual cortex edge perception to morphologically detailed midget ganglion cells. The model replicates local neuronal dynamics as well as edge perception. The suggested model's advantage lies in its similarity to human vision and ability to approximate human vision performance in both night and colour vision. The human scotopic and colour vision models provide a good estimate of true edges. Although the model's ODS performance suffers slightly due to small RFs, it can be enhanced with larger RFs. The use of a larger RF increases computational complexity, which will be discussed in the subsequent sections. The uncoupled model, on the other hand, provides information about the perfect coupling of neuronal fibers in bundled fiber systems for interference-free signal transmission, as well as the most likely configuration for inter-fiber interference. In addition, the bundled fiber interaction model proposes complex coherent signal processing in coupled bundled fiber systems, resulting in controlled amplification or suppression of propagating signals corresponding to neighboring local signals and their associated coupled interaction. The proposed model is based on morphogenesis and the effect of local or non-local aggregated signals on local signal processing. The proposed model is tested using an OS coupled RGC network, which is compared to its uncoupled counterpart. The Histogram of Oriented Gradient data is used to compute the orientation selectivity performance responses, and a comparison of

the two networks shows that the coupled network have more orientation selectivity tuning. The proposed work used to model and simulate local signal dynamics in a bundled fiber system of an OS-RGC network due to cell-field interaction, as well as gain insight into the potential importance of dendritic fiber coupling in orientation selectivity bandwidth adjustment. A similar model focusing on a resilient network could aid researchers in better understanding of both local and global signal processing in the visual cortex and other relevant networks.